Int J Thermophys (2007) 28:1941–1956
DOI 10.1007/s10765-007-0280-1

Thermal Analysis of the Heater-Induced Realization of the Tin Fixed Point

K. Yamazawa · J. V. Widiatmo · M. Arai

Published online: 9 October 2007

Abstract In this article, work concerning the thermal analysis of the tin fixed-point is reported. First, the development of a new fixed-point furnace is described. Improvements in the design of the furnace and in the control system enable measurement of the heater power during the phase change. The furnace is sufficiently thermally insulated to produce excellent uniformity and stability, leading to high quality freeze-initiation and minimal thermal influences on the freezing point. By employing the improved furnace and newly-fabricated tin fixed-point cells, the start and end of the melting plateau and the end of the freezing plateau were accurately determined, enabling reliable evaluation of the liquid fraction during the realization of the tin fixed-point compared to conventional methods. Two open-type tin fixed-point cells were fabricated using high-purity tin that was chemically analyzed for impurity content. Thermal analysis results of freezing-point depression are compared to those based on the chemical analysis.

Keywords Fixed-point furnace · Heater power measurement · Thermal analysis · Tin fixed-point

1 Introduction

Impurities in metal fixed-points cause significant bias to the fixed-point temperature [1–5]. The temperature is affected by the concentration and the distribution of impurities. After a long discussion, CCT WG1 has recommended methodologies to estimate the uncertainty and to correct the fixed-point temperature for the influence of chemical impurities [1]. It is now widely recognized that the SIE (sum of individual estimates)

K. Yamazawa (✉) · J. V. Widiatmo · M. Arai
National Metrology Institute of Japan (NMIJ) AIST, Tsukuba Central 3, 1-1-1 Umezono, Tsukuba, Ibaraki 305-8563, Japan
e-mail: kazuaki-yamazawa@aist.go.jp

method is able to correct the bias due to various impurities, and the OME (overall maximum estimates) is a method to estimate the uncertainty using the first cryoscopic constant. The document also classifies thermal analysis, such as the evaluation of the freezing curves or $1/F$ analysis, as confirmatory methods.

However, we should be aware that the uncertainty estimation and the fixed-point temperature correction are based on uncertain values [2]. The uncertainty of the chemical analysis, employing GDMS or other methods, may be larger than that required by the field of thermometry. The thermometry community must rely on limited reliable data for the distribution coefficient and the slope of the liquidus curve of the dilute binary systems at low concentrations. For fixed-points other than the tin point, for which we have a relatively abundant data set [3], the distribution coefficients and the slopes of the liquidus curves need to be derived by analyzing the binary phase diagrams; otherwise, we are forced to estimate the uncertainty using the OME method.

Furthermore, contamination of the fixed-point substances may occur after the chemical analysis, especially during the fabrication of the cells, so that the apparent uncertainty due to impurities may be greater than that obtained from chemical analysis. Therefore, careful realization of the fixed-point and its analysis are still important.

There are a number of criticisms of the thermal analysis of the melting or freezing plateau. It is difficult to determine accurately the liquid fraction in solid–liquid equilibrium by relying only on the measured temperature. For example, the melt-off point, where the metal has completely melted, may be difficult to determine because the run-off point, where overheated liquid contacts the thermometer well, masks the true liquidus. During solidification, the solid fraction nucleated following supercooling of the liquid metal is likewise difficult to determine. For such reasons, it is generally said that an evaluation based on $1/F$ (F is the liquid fraction) analysis of melting or freezing plateaux is unreliable. As an alternative, the use of adiabatic calorimetry [6–8] or a kind of systematic analysis for F determination [9] is introduced. CCT document CCT/05-08 [1] states that the current state-of-the-art procedure is to adopt the maximum value of the freezing curve as the best approximation, without the necessity of a $1/F$ calculation and analysis.

The authors consider that if a fixed-point apparatus and a realization method enabling an accurate determination of F can be developed, an evaluation using experimental data and related theory can also be conducted accurately. This article will report the development of a new tin furnace, the fabrication of tin fixed-point cells, and thermal analysis based on the measured experimental data.

The development of a new fixed-point furnace is first described. Improvements in the design of the furnace and its control system enable measurement of the heater power during the phase change. By employing the improved furnace, the determination of the start and end of the melting plateau and the end of the freezing plateau can be done accurately, from which reliable evaluation of the tin fixed-point is possible. Two open-type tin fixed-point cells were fabricated in this work using high-purity tin that was chemically analyzed for impurity content. From thermal analysis of the freeze, this article will compare the thermal analysis results to the predictions from the chemical analysis.

2 Apparatus and Method for Accurate $1/F$ Evaluation

2.1 Fixed-Point Furnace

2.1.1 Design of the Fixed-Point Furnace

NMIJ has been developing fixed-point furnaces in recent years. The original tin fixed-point furnace consumed 700 W to maintain the temperature near the tin fixed-point with three zone-heaters, and used water-cooling. Our previous improvements, reported elsewhere [10], to reduce the power consumption and improve the temperature control stability resulted from improving the thermal insulation, with the total heater power consumption being only 50 W and water-cooling is no longer required.

It is well known that the supercooling of the tin fixed-point is deeper than other fixed-point materials [4,5]. Inserting a cold object into the thermometer well and removing the fixed-point cell from the furnace are both common techniques to initiate the freezing plateau. When these methods are employed, however, the amount of material initially solidified is difficult to control. For the furnace reported elsewhere [10], improvement of the temperature control stability under static conditions was achieved, while sacrificing the dynamic response characteristics. For this furnace, the initiation of the tin freezing plateau is done by blowing gas through the thermometer well to obtain highly reproducible nucleation.

In this work, the following further furnace improvements were carried out:

(a) Improvements to the design of the furnace and the control system to enable heater power measurement during the fixed-point realization so that F can be accurately determined,
(b) Improvements in the design of the zone heaters and the internal thermal insulation of the furnace to increase the isothermal region within the metal crucible,
(c) Application of a highly stable control system to ensure high temperature stability during the melting and freezing plateaux, and
(d) Establishment of temperature control for the heater-induced nucleation without the aid of a cold rod or flowing gas, and without the need to remove the fixed-point cell or thermometer.

To implement (a) and (c), a high precision digital PID controller and a stable industrial platinum resistance thermometer (IPRT) were employed for each zone heater. Series-regulated dc power supplies were used to power the heaters. The heater power was calculated from the voltage measurements of each zone heater, $V_i(t)$, and the resistance value of each zone heater, R_i, pre-evaluated in the vicinity of the fixed-point temperature, using the relationship $P(t) = \sum_i \frac{V_i(t)^2}{R_i}$.

To solve (b) and (d), the finite element method (FEM) was employed to simulate the temperature distribution within the furnace, from which the optimal heater power, heater size, positioning of the thermal insulation, and the position of the control sensor can be determined. For simplicity, the furnace was modeled in two dimensions, taking advantage of the axial symmetry.

The heating system consists of three independent zone heaters. To obtain good uniformity during heating and cooling, we designed the internal structure in such a way

that the isothermal lines in the vicinity of the crucible become parallel. Furthermore, the furnace must have good dynamic response to be capable of heater-induced fixed-point realization. Minimization of the heat capacity of the parts within the furnace during the design phase ensured good dynamic response.

2.1.2 Characteristics of the Furnace

When realizing the freezing plateau of a metal fixed-point, a thermal flux from the sensor to ambient will occur and the thermometer will not be in thermal equilibrium with the interface if the liquid–solid interface does not adequately surround the thermometer sensing element. On the other hand, when the thermometer sensing element is nearly entirely surrounded by a liquid–solid interface and an infinitely small thermal flux is present between the liquid–solid interface and its surroundings, the thermometer sensing element will be in quasi-thermal equilibrium with the liquid–solid interface. Furthermore, if we ensure that the thermal flux from the interface to the surroundings is constant, we can maintain a constant rate of phase change. Under this quasi-thermal equilibrium with a small constant heat flow, thermal analysis of the melt or freeze should be possible.

Our objective in this article is to develop a fixed-point furnace that enables thermal analysis. Such a furnace requires a large isothermal region within the crucible to ensure a uniform phase transition and a highly stable furnace temperature to ensure a steady heat flow. To accurately measure the heat required during a phase transition, a nonstandard nucleation procedure was used; i.e., the nucleation was induced by only adjusting the furnace temperature. To initiate a heater-induced nucleation that enables an accurate estimate of the initially solidified fraction, a satisfactory dynamic response of the furnace to changes of the programmed temperature is necessary.

Measurements along the thermometer well with the tin sample in the solid phase were done to optimize the temperatures of the three zone heaters. After this optimization, the temperature distribution along the thermometer well of the fixed-point was within 2 mK. The adoption of IPRTs as control sensors for the feedback loops produce a satisfactory stability within $\pm$ 2 mK during a 24 h interval. Such stability is adequate, since experimental work described later deals with $\Delta T_{\text{setting}}$ between 0.2 to 3 K, where $\Delta T_{\text{setting}}$ is $|T_{\text{setting}} - T_{\text{Sn}}|$, while T_{Sn} and T_{setting} are temperatures close to the tin freezing point and the desired final furnace temperature, respectively.

A test was executed to evaluate the response of the furnace. The results showed that the furnace responds perfectly to the programmed temperatures at a slope of $\pm$ 0.2 K$\cdot$ min^{-1}. The feedback control developed in this work makes use of the temperature value at the control sensor to produce the programmed temperature. A systematic delay of approximately 15 min was observed; however, the rate of the temperature change is very reproducible. Furthermore, the programmed temperature-difference is also satisfactorily reproduced; for example, a 10 K temperature difference was realized within 2 mK.

The key point of this article is that, as a novel procedure, the heater power is measured during the fixed-point realization so that the energy required for the phase transition and the phase transition termination points can be determined. There should be a strong correlation between the temperature setting and the heater power that makes

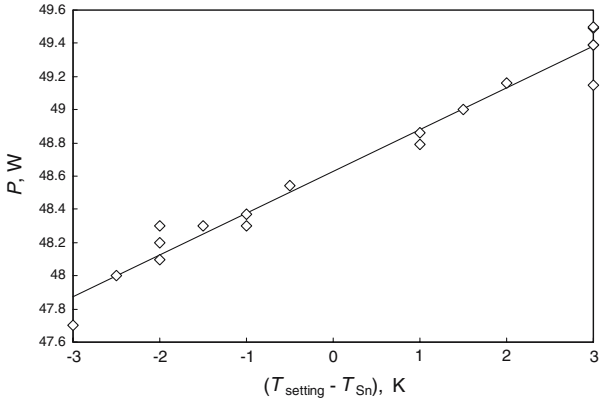

Fig. 1 Heater power versus temperature setting

this method practical. Figure 1 shows the heater power in terms of the temperature setting. The abscissa is the departure of temperature equivalent to the temperature of the heater, T_{setting}, from the tin freezing point, T_{Sn}. The total heater power, P, summed up for the three zone heaters under steady-state conditions at the tin freezing point temperature is approximately 48.6 W. The deviation of the heater power was only approximately 1 W for $(T_{\text{setting}} - T_{\text{Sn}}) = \pm 3\,\text{K}$; however, strong linearity between $(T_{\text{setting}} - T_{\text{Sn}})$ and P was confirmed. This implies that, by using the new furnace system, the energy required for the phase transition, along with the termination points of the phase transition, can be easily determined due to the highly reproducible heat loss of the furnace itself; the amount of excessive heat consumption directly reflects the power required for the phase transition of the fixed-point metal.

All the characteristics presented here show the success of the application of FEM in the design of our new furnace, and we are confident that it is suited to conducting thermal analysis of tin melting and freezing plateaux.

2.2 Fixed-Point Cell

Fixed-point cells used in this study consist of a graphite crucible and a graphite cap, within which the tin ingot is enclosed; a graphite thermometer well and its graphite holder, fixing the well in the center of the crucible; a quartz thermometer well that is placed in the graphite thermometer well; graphite wool, acting as a heat insulator; a quartz cylinder that encloses all those parts; and the cylinder cap, sealing the inner part of the quartz cylinder. The cylinder cap is equipped with a gas port, enabling pressurization or evacuation of the cylinder. The graphite parts were of 5N nominal purity (Toyo Tanso) and baked in vacuum at least 100 h at 980°C.

A single tin rod sized 32 mm in diameter and 200 mm in length was used to fabricate one tin cell using a metal filling method reported elsewhere [11]. Two cells were fabricated, one using 6N nominal purity tin rod (Cell Sn No. 4, Specimen Lot No. 6NSn050404) and the other 5N (Cell Sn No. 6, Specimen Lot No. SnC0502-2). The tin rods were analyzed by the manufacturer using GDMS. The purity of the metal used

in Cell Sn No. 4 is the highest level available commercially. Although the 5N-purity tin cell is not used for calibrations, the use of cell Sn No. 6 allows high and lower-level purity metals to be compared.

2.3 Measurement System

A resistance bridge (ASL model F900) coupled with an external 100 Ω standard resistor (Tinsley Model 5648) was employed in this work to measure the SPRT (Chino Model R800-2) resistance. The temperature measurements during the melting plateau and the following freezing plateau were conducted as one experimental run. Between the runs, the resistances of the SPRT at the triple point of water and the gallium point were measured to confirm the stability of the SPRT.

2.4 Fixed-Point Realization Method

The tin fixed-point was realized by freezing tin that had been completely melted. The freezing process is often induced by inserting a rod into the quartz thermometer well, causing nucleation to take place on the wall of the thermowell. In this work, a nonstandard method whereby nucleation was initiated by changing the furnace temperature was used in order to measure the amount of heat required for the phase transition; the solid–liquid interface is expected to begin at the crucible wall and to move inward towards the thermowell as solidification progresses.

To initiate nucleation, the following procedure was carried out. Each zone heater applies the procedure based on its optimum setting as predetermined by minimizing the vertical temperature gradient in the fixed-point cell. The nucleation was started from a temperature of $T_{\mathrm{Sn}} + 3\,\mathrm{K}$, where T_{Sn} is the optimum temperature of each zone near the tin freezing point.

1. Reduce the furnace temperature from $T_{\mathrm{Sn}} + 3\,\mathrm{K}$ down to $T_{\mathrm{Sn}} - 12\,\mathrm{K}$ at a rate of $0.2\,\mathrm{K}\cdot\mathrm{min}^{-1}$, during which supercooling occurs, followed by recalescence.
2. Maintain the temperature at $T_{\mathrm{Sn}} - 12\,\mathrm{K}$ for 15 min, and then increase it to $T_{\mathrm{setting}} - 0.5\,\mathrm{K}$ at a rate of $0.2\,\mathrm{K}\cdot\mathrm{min}^{-1}$.
3. Change the temperature to T_{setting}, at a rate of $0.02\,\mathrm{K}\cdot\mathrm{min}^{-1}$.

The above procedure produces the best tin freezing curve with minimal overshoot. Figure 2 shows the temperature profile obtained, along with the beginning of the freezing plateau, as measured by a SPRT. As shown in Fig. 2, the temperature decreases and nucleation occurs within the cell; then, the temperature setting is raised to the T_{setting} in a manner not to overshoot the T_{setting}.

Measurements to confirm the repeatability of temperature during the tin solidification were made using cell Sn No. 4 at $T_{\mathrm{setting}} = T_{\mathrm{Sn}} - 2\,\mathrm{K}$. The measurements were repeated ten times at the same point within the plateau realization, namely 60 min following the recalescence, to produce ten data plots as given in Fig. 3. Measurements were carried out using two currents, from which the measured values were extrapolated to zero current. The ordinate of Fig. 3 shows the deviation of the zero-current values, $W_{0\mathrm{mA}}$, from their average, $W_{0\mathrm{mA,\ ave}}$. The standard uncertainty of the measured

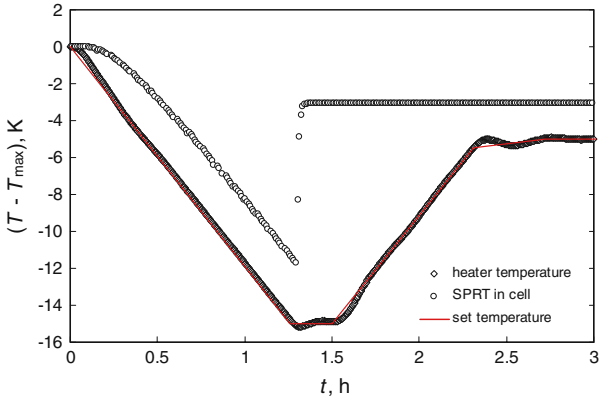

Fig. 2 Control profile of the furnace during the realization of the freezing point of tin

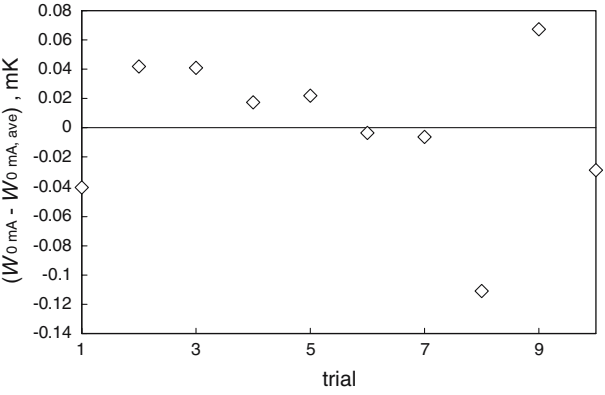

Fig. 3 Reproducibility of the resistance ratio during the freezing plateau of cell Sn No. 4; plateau measurements were repeated ten times at $T_{\text{setting}} = T_{\text{Sn}} - 2\,\text{K}$

data was 0.02 mK. This confirms the satisfactory reproducibility of the heater-induced realization method using the present furnace.

3 Experiments and Discussion

3.1 Profile of the Heater Power during the Fixed-Point Realization

Figure 4a and b show the measurement results during the melting and freezing plateaux, respectively. In each figure, the total heater power summed from the three zone heaters is shown along with the temperature measured within the fixed-point cell.

At the beginning of the melting plateau, the heater power is high, since power is required to heat the parts within the furnace as a consequence of their heat capacities. After this transient change, the heater power becomes stable until the 550 min point, where the heater power is slightly higher than the steady-state power consumption,

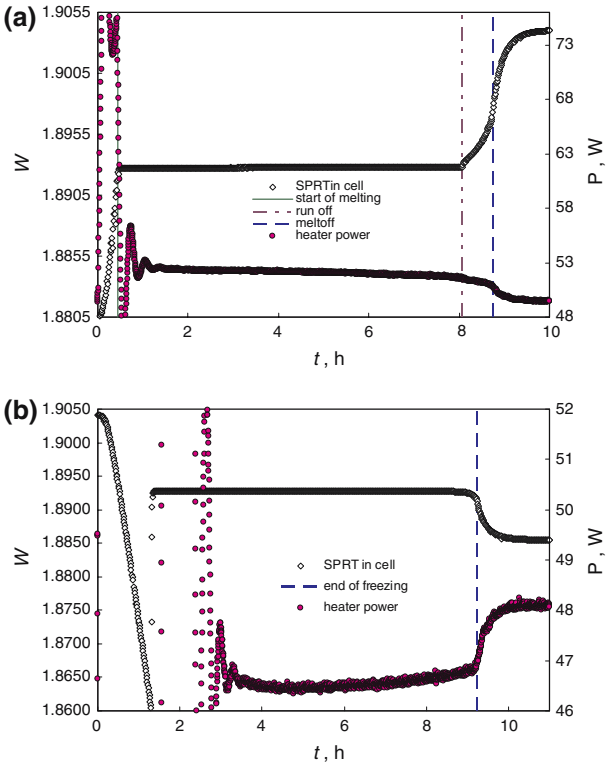

Fig. 4 Relation of the melting/freezing plateau to the heater power: (**a**) during the melting plateau and (**b**) during the freezing plateau

49.5 W, required to maintain $T_{\text{setting}} = T_{\text{Sn}} + 3\,\text{K}$. On the melting curve formed by the heater power in Fig. 4a, there are two points at which the slope of the curve changes. From comparison with the simultaneous temperature measurement, these two points correspond to the "run off" and the "melt off" points, respectively [6].

As shown in Table 1, the amount of metal within the fixed-point cell crucible is approximately 10 mol. The integral of the excess heater power is 70 kJ, which coincides with the value required to melt all of the metal within the crucible, calculated from the literature value ($7.07\,\text{kJ}\cdot\text{mol}^{-1}$) for the heat of fusion [12].

Figure 4b shows the heater profile during the realization of the freezing plateau for $T_{\text{setting}} = T_{\text{Sn}} - 2\,\text{K}$. The fluctuation of the heater power is large for the first 200 min

Table 1 Tin fixed-point cells studied in the present work

Cell	Mass of ingot (g)	Size	Nominal purity	Supplier
Sn No. 4	1176	Φ32×L200	6N	NM[a]
Sn No. 6	1176	Φ32×L200	5N	NM

[a] Nippon Mining & Metals Co. Ltd

of the nucleation procedure (see Sect. 2.2). However, the heater power becomes stable at a power obviously lower than 48 W, which is the steady-state power for $T_{\text{setting}} = T_{\text{Sn}} - 2\,\text{K}$. The change in the slope of the heater power curve indicates the termination of the freezing plateau. Furthermore, by integrating the heater power, we can calculate the fraction of liquid (F) at any point of the freeze. Measurements similar to that in Fig 4b were done for many $\Delta T_{\text{setting}}$ values, with the lowest being $T_{\text{setting}} = T_{\text{Sn}} - 0.5\,\text{K}$ where, during a 33-h plateau, the change in the power profile was small, but still observable.

From the heater power curve, it is possible to identify the key parameters required for thermal analysis, namely, the "melt off" point of the melting plateau and the termination of the freezing plateau. Some literature reports evaluate the liquid fraction by using parameters such as the "run off" point [6] or by defining the termination point by a certain criterion [9]; however, such definitions do not reflect the physical status of the entire cell and would result in misinterpretation of the liquid fraction. In contrast, our solution leads to more accurate thermal analysis.

3.2 Thermal Analysis of the Freezing Plateau

Following the nucleation procedure in Sect. 2.2, the time required for the phase change (phase-change time) was measured for both melting and freezing. Considering the satisfactory realization of the programmed temperature by the furnace, it is possible to estimate the effect of the nucleation procedure on the phase-change time for freezing. Figure 5 represents the phase-change time, $t_{\text{phasechange}}$, measured at various T_{setting} values using two tin cells in the new furnace. The legend of the figure identifies the cells used and the condition under which the measurements were done, namely, during melting (closed symbols) or freezing (open symbols). The line shows the tendency of the data plots. The data plot with open symbols is obtained after converting the programmed temperature for the initial nucleation (see Fig. 2) by assuming that the entire plateau was realized at a constant temperature of T_{setting}. The similarity of the open data plots in Fig. 5 to the closed ones shows the consistency of this conversion. Since the two cells in Fig. 5 have tin of the same mass and identical cell design, they show very similar behavior. Figure 5 also shows that $t_{\text{phase change}}$ is inversely proportional to $\Delta T_{\text{setting}}$. In other words, $\Delta T_{\text{setting}}$ directly reflects the rate of solidification.

In the present work, the phase change is carried out by fixing each zone heater temperature some degrees above (melting) or below (freezing) the tin freezing point. Since all zone heaters used the common procedure described in Sect. 2.2, as shown in Fig. 4, the same amount of heat is constantly added to (or removed from) the tin by the heaters for almost the entire time of the phase transition, implying that the mass of tin is melted (or frozen) at a constant rate. From this, the fraction of liquid tin, usually denoted by F, can be approximated by the ratio of the elapsed time from the initiation of the phase change to the total time required for the complete phase change, insofar as the times of initiation and termination are clearly defined.

A typical freezing curve is shown in Fig. 6, where the resistance ratio of the resistance thermometer used, W, is displayed versus inverse liquid fraction, $1/F$. Figure 6a shows the result for the high purity cell, Sn No. 4. The plot starts from the point

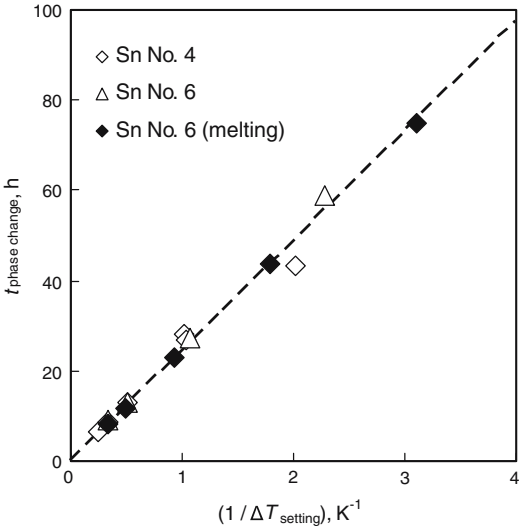

Fig. 5 Phase change time during melting and freezing

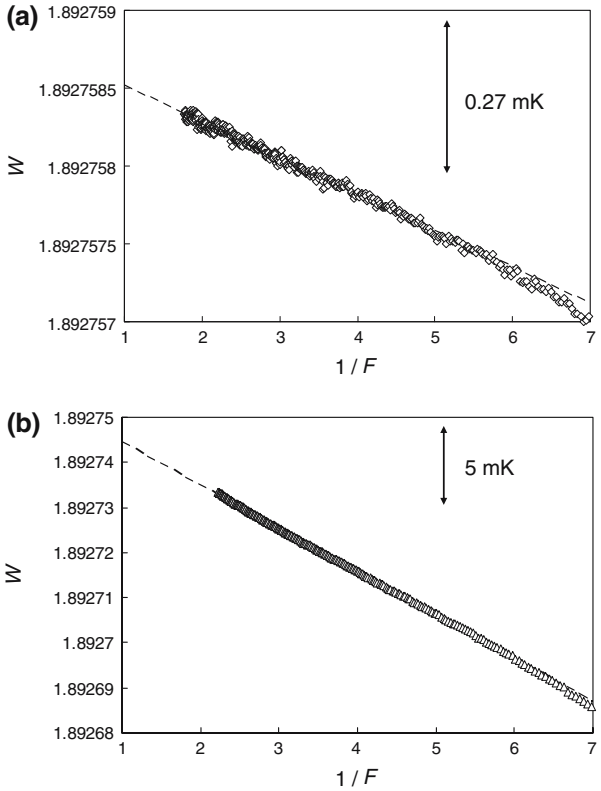

Fig. 6 Freezing curve at the tin fixed-point: (**a**) cell Sn No. 4 and (**b**) cell Sn No. 6

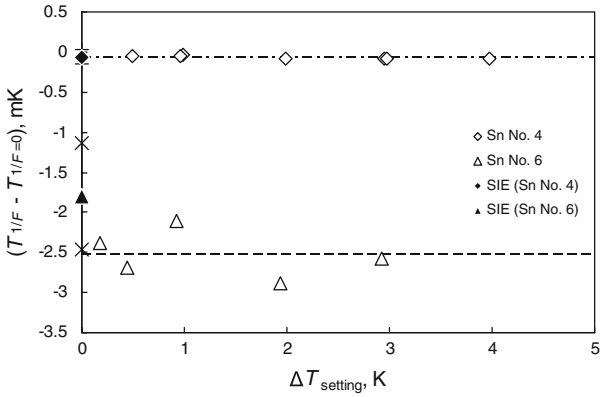

Fig. 7 Comparison of thermal analysis and the SIE

at which the temperature recalescence finished. Since the nucleation was initiated by keeping the heater temperature significantly lower than the tin point for a relatively long period, the first solid mantle formed occupied nearly 50% of the volume. After this, the freezing curve forms a straight line up to $1/F = 5$ (a straight-line fit to the data in Fig. 6a) before the tin completely solidifies. For convenience, the gradient of this straight line is termed here the slope of the freezing curve. Figure 6b shows a similar plot for the low purity cell, Sn Cell No. 6. Even with this purity, we can confirm from the experimental data that the $1/F$ plot is a straight line, in accordance with the theory described in the following subsection. It should be noted that there was a three-month interval between the measurements shown in Fig. 6a and those in Fig. 6b, during which the measuring SPRT had drifted $+0.4$ mK at the TPW. Simple comparison between resistance ratios shown in Fig. 6a and b would consequently cause misinterpretation of the data, and we decided to treat each freezing curve individually in the analysis presented below.

Since measurements at various rates of solidification, as reflected by the $\Delta T_{\text{setting}}$ values, were carried out in conjunction with this work, it is possible to examine the dependence of the slope of the freezing curves on the rate of solidification, as shown in Fig. 7. The data distribution, especially for cell Sn No. 4 in Fig. 7, implies that the slope of the freezing curve, $\mathrm{d}T/\mathrm{d}(1/F)$, does not depend on the rate of solidification. The figure also shows that the slope reflects the quality (purity) of the cell, namely, the cell with the higher nominal purity (Sn No. 4) has a smaller slope than that of the lower purity cell (Sn No. 6). The slope of the freezing curve is often used as a measure of the quality of the cell. As shown in Fig. 7, the measured slopes form a relatively wide band for the cell of lower purity, Sn No. 6, implying that measurements for thermal analysis should be carried out over a wide range of furnace temperature settings.

3.3 Comparison with the Chemical Analysis

The manufacturer provided impurity analyses for each tin sample using GDMS (Y. Shindo, personal communication). Table 2 lists the impurity elements detected.

Table 2 Impurities in tin fixed-point cells studied in the present work (Y. Shindo, personal communication)

Element	Sn No. 4 mass (ppm)	Sn No. 6 mass (ppm)	$\partial T/\partial c_{li}$ (mK/at %)	$k_{0,i}$
Li	<0.01	<0.01	−2	0.01
B	<0.01	<0.01		
C	<10	<10		
N	<10	<10		
O	<10	<10		
Na	<0.01	<0.01	−2.89	0.36
Mg	<0.01	<0.01	−2.45	0.053
Al	<0.01	<0.01	−1.69	0.25
Si	<0.01	<0.01	−2.67	0.1
P	<0.01	<0.01		
S	0.02	<0.01		
Cl	<0.01	0.07		
K	< 0.01	<0.01		
Ca	<0.01	<0.01	−2.9	0.02
Ti	<0.01	<0.01	−2.39	0.06
V	<0.01	<0.01		
Cr	<0.01	0.09		
Mn	<0.01	<0.01		
Fe	<0.01	1.6	−2.87	0.03
Co	<0.01	<0.01	−0.34	
Ni	<0.01	0.06	−2.95	0.042
Cu	0.07	1	−3.97	0.021
Zn	<0.01	<0.01	−3.43	0.083
Ga	<0.01	<0.01	−2.28	0.16
Ge	<0.01	<0.01	−1.39	0.53
As	<0.01	0.17	−0.71	0.76
Zr	<0.01	<0.01		
Nb	<0.01	<0.01		
Mo	<0.01	<0.01		
Ag	0.05	<0.1	−2.84	0.036
Cd	<0.05	<0.05	−2.27	0.28
Sb	<0.5	<0.5	2.93	2.167
Ba	<0.01	<0.01		
W	<0.01	<0.01		
Au	<0.05	<0.05	−2.87	0.039
Pb	<0.01	<0.01	−2.79	0.098
Bi	<0.01	<0.05	−2.16	0.27
Th	<0.005	<0.005		
U	<0.005	<0.005		

Using the values listed in Table 2, it is possible to estimate the departure of the realized tin freezing temperature from the ideal one. A recommended estimation method is the SIE [1–3], given in Eq. 1, that shows the dependence of the observed equilibrium freezing temperature, T_{obs}, on the liquid fraction, F.

$$T_{\mathrm{obs}} - T_{\mathrm{pure}} = \sum_i c_{\mathrm{l}i} \left(\frac{\partial T}{\partial c_{\mathrm{l}i}} \right) F^{k_{0,i}-1} = \sum_i c_{\mathrm{l}i} \left(\frac{\partial T}{\partial c_{\mathrm{l}i}} \right) \left(\frac{1}{F} \right)^{1-k_{0,i}}, \qquad (1)$$

T_{pure} in Eq. 1 denotes the freezing temperature of the ideally pure fixed-point metal, and c_{li}, $(\partial T/\partial c_{\text{li}})$, and $k_{0,i}$ are the concentration of impurity i in equilibrium liquid, the slope of the liquidus line in phase diagram with respect to c_{li}, and the equilibrium distribution coefficient of i, respectively. Since the liquidus point is defined as the equilibrium freezing temperature at $F = 1$, Eq. 1 yields Eq. 2 for the SIE and Eq. 3 for the standard uncertainty of the SIE.

$$\Delta T_{\text{SIE}} = \sum_i c_{\text{li}} \left(\frac{\partial T}{\partial c_{\text{li}}} \right), \tag{2}$$

$$u^2 \left(\Delta T_{\text{SIE}} \right) = \sum_i \left(\left[u \left(c_{\text{li}} \right) \left(\frac{\partial T}{\partial c_{\text{li}}} \right) \right]^2 + \left[c_{\text{li}} u \left(\frac{\partial T}{\partial c_{\text{li}}} \right) \right]^2 \right), \tag{3}$$

The data of $\partial T/\partial c_{\text{li}}$ for employing Eqs. 2 and 3 are taken from the report by Fellmuth and Hill [3]. The standard uncertainty of the ΔT_{SIE}, $u(\Delta T_{\text{SIE}})$, can be calculated following the method also proposed by Fellmuth and Hill [3], where half of the concentration values or half of the detection limit are taken as the uncertainties of the analysis results, $u(c_{\text{li}})$, and a relative uncertainty of order 20% for $u(\partial T/\partial c_{\text{li}})$, which results from the difference between the calculated phase diagrams and the experimental values. Table 3 shows the SIE for the present tin cells along with their standard uncertainties.

Since, as described in the previous subsection, the slope of the freezing curve also reflects the quality of the cell, it is of interest to see how much this slope departs from the SIE. This evaluation using the slope of the freezing curve is termed 'thermal analysis' for convenience.

The slope of the freezing curve (at $F = 1$) can be derived from Eq. 1 to obtain Eq. 4.

$$\left[\frac{\partial \left(T_{\text{obs}} - T_{\text{pure}} \right)}{\partial \left(1/F \right)} \right]_{F=1} = - \sum_i c_{\text{li}} \left(k_{0,i} - 1 \right) \left(\frac{\partial T}{\partial c_{\text{li}}} \right), \tag{4}$$

The slope of the freezing curve, $\partial(T_{\text{obs}} - T_{\text{pure}})/\partial(1/F)$, represented by Eq. 4, differs from Eq. 2 for the SIE by a factor $-(k_{0,i} - 1)$. It will always be negative, since for $k_{0,i} < 1$, $\partial T/\partial c_{\text{li}} < 1$, while for $k_{0,i} > 1$, $\partial T/\partial c_{\text{li}} > 1$. Accordingly, for samples with only $k_{0,i} > 1$ elements, the thermal analysis will give a false result, i.e., values with opposite sign to the SIE. For tin binary systems, only antimony (Sb) elevates the freezing point ($k_{0,i} > 1$), but its concentration in our tin samples is below the GDMS detection limit.

Table 3 ΔT_{SIE} and slope of the freezing curves for the tin fixed-point cells studied in the present work

Cell	ΔT_{SIE} (mK)	$u(\Delta T_{\text{SIE}})$ (mK)	$\partial(T_{\text{obs}} - T_{\text{pure}})/\partial(1/F)$ (mK)	$u(\partial(T_{\text{obs}} - T_{\text{pure}})/\partial(1/F))$ (mK)
Sn No. 4	−0.068	0.086	−0.066	0.102
Sn No. 6	−1.80	0.67	−1.73	0.71

Table 3 also lists the value of $\partial(T_{\text{obs}}-T_{\text{pure}})/\partial(1/F)$, calculated from Eq. 4 and Table 2, and its uncertainty. In relation to both tin cells, $\partial(T_{\text{obs}} - T_{\text{pure}})/\partial(1/F)$ is almost identical to the SIE values, the difference between them being within the uncertainty.

The comparison of the thermal analysis and the SIE (closed symbol) is depicted in Fig. 7. Error bars |-| and ×–× in Fig. 7 correspond to $\pm u(\Delta T_{\text{SIE}})$ of cells Sn No. 4 and Sn No. 6, respectively. The thermal analysis agrees satisfactorily with the SIE for cell Sn No. 4. For cell Sn No. 6, the thermal analysis shows great departure from the SIE; however, the average value (broken line) is almost within the uncertainty of the SIE.

3.4 Comparison with the Direct Cell Comparison

Both the thermal analysis and the SIE have shown that cell Sn No. 4 has greater purity than cell Sn No. 6. From the thermal analysis, it is also possible to estimate the temperature difference between the cells by considering the difference in the slopes of their freezing curves. However, since the thermal analysis was applied individually to each cell and considering that the measuring SPRT may drift during the measurements of an individual cell, this should also be confirmed by direct comparison. One additional furnace was introduced and, during the simultaneous realization of the two fixed points, the temperature difference was determined using two sets of SPRTs and resistance bridges, exchanging them in intervals for the direct cell comparison.

Figure 8 presents the cell comparison results. $T_{1/F}$ in the ordinate of Fig. 8 is temperature measured at any F and corresponds to T_{obs} in Eq. 1, while $T_{1/F=0}$ corresponds to T_{pure}. For thermal analysis, $T_{1/F=0}$ is determined from $T_{1/F=0} = T_{1/F=1} - \partial T/\partial(1/F)$, in which $\partial T/\partial(1/F)$ is the slope of the freezing curve obtained from thermal analysis. The direct cell comparison results, derived from $(T_{\text{Sn No. 6}})_F = (T_{\text{Sn No. 4}})_F - (T_{\text{cell comp.}})_F$, where $(T_{\text{Sn No. 4}})_F$, $(T_{\text{Sn No. 6}})_F$, and $(T_{\text{cell comp.}})_F$, which are the temperature of cell Sn No. 4, the temperature of cell Sn No. 6, and the temperature difference between the cells, respectively, measured at any F, are plotted as open circles. For comparison, the freezing curves of cells Sn No. 4 and Sn No. 6

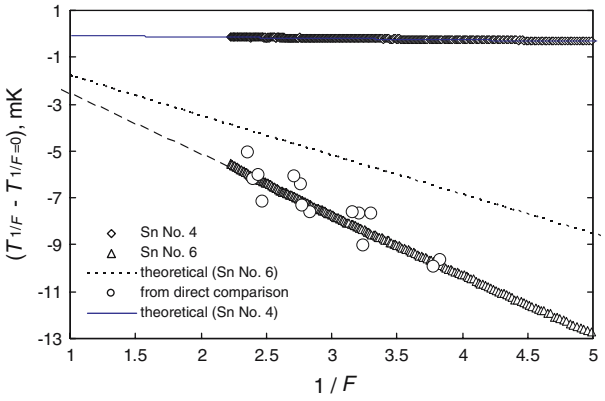

Fig. 8 Direct comparison between cells Sn No. 4 and Sn No. 6

obtained from individual plateau measurements are shown together. Despite the scatter of the direct comparison data, $(T_{\text{Sn No. 6}})_F$ agrees well with the freezing curve of cell Sn No. 6. This agreement implies that the thermal analysis of individually measured freezing curves is a reliable means to estimate the temperature differences among cells.

Also shown in Fig. 8 are the theoretical freezing curves derived from Eq. 1 for cells Sn No. 4 and Sn No. 6. For cell Sn No. 4, the experimental freezing curve almost overlaps the theoretical one, indicating satisfactory agreement between experiment and theory. On the other hand, the experimental freezing curve of cell Sn No. 6 deviates from the theoretical one. A fact that should be noted is that both theoretical freezing curves are straight lines. $(T_{\text{Sn No. 6}})_F$, determined experimentally, also shows a tendency to change linearly as a function of $1/F$. We believe that this linear tendency shows the accordance of the experimental results with the theory described by Eq. 1. However, the experimental results obviously deviate from the theoretical line calculated by substituting the values in Table 2 into Eq. 1. The result for cell Sn No. 6 is considered to be due to some impurities that were not detected by the GDMS analysis, and shows the risk of relying exclusively on the SIE, and at the same time illustrates the importance of accurate thermal analysis.

4 Conclusion

An improved tin fixed-point furnace has been developed which allows the heater power consumed during the phase change of tin to be measured. This very high quality furnace with satisfactory thermal insulation that produces excellent uniformity and stability has led to a high quality freeze with minimal thermal influences. From the evaluation of the newly developed tin furnace, the potential of the heater power measurement as additional input to the thermal analysis was confirmed. The method proposed here enables an accurate determination of $1/F$ compared to conventional methods. Two tin fixed-point cells were also newly fabricated from two different sources (cell Sn No. 4 of 6N purity and cell Sn No. 6 of 5N purity). From the comparison of the temperature measured by a thermometer within the fixed-point cell with the measured heater power, the precise determination of the termination of the phase change, especially the run-off and melt-off points, essential to thermal analysis was successfully achieved. The good agreement between the thermal analysis and the SIE for cell Sn No. 4 may reflect the reliability of thermal analysis for estimating the influence of impurities on the realization of the tin point. On the contrary, the result of cell Sn No. 6 shows the risk of relying solely on the SIE, and at the same time illustrates the importance of accurate thermal analysis.

Acknowledgments The authors are indebted to Mr. Yuichiro Shindo from Nippon Mining & Metals Co., Ltd. (the former body was Nikko Materials Co., Ltd.) for providing the 5N grade single tin rod along with its impurity analysis. The rod enabled the fabrication of one of the cells used in the present work.

References

1. D. Ripple, B. Fellmuth, M. de Groot, Y. Hermier, K.D. Hill, P.P.M. Steur, A. Pokhodun, M. Matveyev, P. Bloembergen, CCT Document CCT/05-08 (2005)

2. K.D. Hill, S. Rudtsch, Metrologia **42**, L1 (2005)
3. B. Fellmuth, K.D. Hill, Metrologia **43**, 71 (2006)
4. J.J. Connolly, J.V. McAllan, Metrologia **16**, 127 (1980)
5. G.T. Furukawa, J.L. Riddle, W.G. Bigge, E.R. Pfieffer, NBS Spec. Pub. 260–77 (1982)
6. J. Ancsin, Metrologia **38**, 1 (2001)
7. G. Bonnier, E. Renaot, Metrologia **33**, 363 (1996)
8. E. Renaot, M. Elgourdu, G. Bonnier, in *Proceedings TEMPMEKO 99, 7th Int. Symp. on Temperature and Thermal Measurements in Industry and Science*, ed. by J. Dubbeldam, M. de Groot. (Edauw Johannissen bv, Delft, 1999), pp. 119–123
9. G.F. Strouse, CCT Document CCT 03-19
10. J. Tamba, K. Sato, K. Yamazawa, I. Kishimoto, M. Arai, Trans. SICE **41**, 187 (2005) [in Japanese]
11. J.V. Widiatmo, K. Harada, K. Yamazawa, M. Arai, Metrologia **43**, 561 (2006)
12. *Rika Nenpyo* (Chronological Scientific Tables), National Astronomical Observatory, Maruzen Co., Ltd., ISBN4-621-04927-5